Quantitative photoacoustic assessment of red blood cell aggregation under pulsatile blood flow: experimental and theoretical approaches

Tae-Hoon Bok, Eno Hysi, Michael C. Kolios*
Department of Physics, Ryerson University, 350 Victoria Street, Toronto, Ontario, M5B 2K3, Institute for Biomedical Engineering, Science and Technology, a partnership between Ryerson University and St. Michael's Hospital, Keenan Research Center for Biomedical Sciences of St. Michael's Hospital, 209 Victoria Street, Toronto, Ontario, M5B 1T8, Canada;

ABSTRACT

In the present paper, the optical wavelength dependence on the photoacoustic (PA) assessment of the pulsatile blood flow was investigated by means of the experimental and theoretical approaches analyzing PA radiofrequency spectral parameters such as the spectral slope (SS) and mid-band fit (MBF). For the experimental approach, the pulsatile flow of human whole blood at 60 bpm was imaged using the VevoLAZR system (40-MHz-linear-array probe, 700-900 nm illuminations). For the theoretical approach, a Monte Carlo simulation for the light transmit into a layered tissue phantom and a Green's function based method for the PA wave generation was implemented for illumination wavelengths of 700, 750, 800, 850 and 900 nm. The SS and MBF for the experimental results were compared to theoretical ones as a function of the illumination wavelength. The MBF increased with the optical wavelength in both theory and experiments. This was expected because the MBF is representative of the PA magnitude, and the PA signal from red blood cell (RBC) is dependent on the molar extinction coefficient of oxyhemoglobin. On the other hand, the SS decreased with the wavelength, even though the RBC size (absorber size which is related to the SS) cannot depend on the illumination wavelength. This conflicting result can be interpreted by means of the changes of the fluence pattern for different illumination wavelengths. The SS decrease with the increasing illumination wavelength should be further investigated.

Keywords: photoacoustics, red blood cell aggregation, Monte-Carlo simulation, spectral parameter, optical wavelength dependence

1. INTRODUCTION

The photoacoustic (PA) signal amplitude, under conditions of constant fluence, is dependent on the optical absorption coefficient (μ_a) and the absorber size[1]. Recently, our group has investigated how PA imaging can simultaneously assess the changes in red blood cell (RBC) aggregation and oxygen saturation (sO_2) under pulsatile blood flow conditions[2–4]. The PA signal amplitude and sO_2 varied cyclically with the beat rate of the pulsatile flow but out of phase with one another. In this paper, we investigate the effect of the optical wavelength of illumination on the magnitude of the cyclical variation of the PA signal.

The objective of the work is two-fold: first, given the clinical significance of the functional sO_2 PA imaging using[5], it is important to understand the role that the wavelength of illumination plays during realistic blood flow conditions. This will enable more accurate sO_2 estimates and potentially improve the sensitivity of PA imaging, as it prepares for making impactful clinical transitions. Secondly, this work utilizes radiofrequency (RF) PA spectroscopy[6,7], a recently developed technique that aims for extracting relevant, system-independent parameters that used for tissue characterization. In the context of imaging blood flow using acoustic-resolution PA imaging systems, RF spectroscopy could provide assessments of effective absorber size and shape. This is particularly important in conditions related to RBC aggregation such as diabetes and deep vein thrombosis[8,9].

* mkolios@ryerson.ca

Photons Plus Ultrasound: Imaging and Sensing 2017, edited by Alexander A. Oraevsky, Lihong V. Wang, Proc. of SPIE Vol. 10064, 100645F · © 2017 SPIE · CCC code: 1605-7422/17/$18 · doi: 10.1117/12.2250221

2. MATERIALS AND METHODS

2.1 Experimental approach - human blood PA imaging

Human blood was collected by netCAD, the research division of Canadian Blood Services (Vancouver, BC, Canada), under protocol 2013-001. The procedures for using the blood have been approved by the research ethics boards of Ryerson University and the Canadian Blood Services. Whole blood units from three different volunteers were used to ensure the repeatability of experimental results. The PA image of flowing blood was acquired by an ultrasound(US)/PA imaging system (VevoLAZR, FUJIFILM VisualSonics, Toronto, ON, Canada)) equipped with a 40 MHz linear-array probe (LZ550, FUJIFILM VisualSonics, Toronto, ON, Canada) under an experimental flow system. The probe was tilted slightly in order to measure the blood flow velocity as well as the PA signals at the same setup as shown in Figure 1a. PA measurements were performed at 21 optical wavelengths (λ) from 700 nm to 900 nm every 10 nm under 60 bpm of beat rate. The PA B-mode frames, corresponding to a measurement time of 10 seconds at a 20 fps frame rate (a total 200 frames), were recorded at each wavelength. Detailed procedures were described in our previous study[4].

2.2 Theoretical approach - Monte Carlo & PA simulation

In order to validate the experimental results, theoretical models were developed using the mcxyz,c Monte Carlo simulation package for the light propagation through the multi-layered media[10–12] and using the Green's function based method for modeling the PA wave generation[13,14].

When a laser pulse illuminates a medium with a fluence $F(\mathbf{x})$, the energy absorbed by the medium at position $\mathbf{x}$ is:

$$W(\mathbf{x}) = \mu_a(\mathbf{x})F(\mathbf{x}), \tag{1}$$

where, $\mu_a(\mathbf{x})$ is the optical absorption coefficient of the medium. A source of initial excess pressure will be generated in the medium under the condition of thermoelastic stress confinement[1], where the thermal conduction and stress propagation are ignored, and the pressure is expressed by:

$$p_0(\mathbf{x}) = \frac{\beta(\mathbf{x})c^2(\mathbf{x})}{C_p(\mathbf{x})}W(\mathbf{x}), \tag{2}$$

where, $\beta(\mathbf{x})$ is the thermal expansion coefficient, c is the sound speed and $C_p(\mathbf{x})$ is the specific heat capacity.

When the laser pulse length is shorter than the thermal relaxation time, and the medium is homogeneous with a constant sound speed, the PA wave propagation is described by the differential equation:

$$\left(\frac{\partial^2}{\partial t^2} - c^2\nabla^2\right)p(\mathbf{x},t) = p_0(\mathbf{x})\frac{\partial}{\partial t}\delta(t), \tag{3}$$

where $p(\mathbf{x},t)$ is the PA wave pressure and $\delta(t)$ is the Dirac impulse function. The forward solution for the PA wave pressure is given by[15]:

$$\begin{aligned} p(\mathbf{x},t) &= \frac{1}{c^2}\frac{\partial}{\partial t}\int g(\mathbf{x}-\mathbf{x}',t)p_0(\mathbf{x}')d\mathbf{x}', \\ \text{where } g(\mathbf{x},t) &= \frac{\delta(\|\mathbf{x}\| - ct)}{4\pi\|\mathbf{x}\|} \quad \text{(Green's function)} \end{aligned} \tag{4}$$

The 3-D structure of illuminated area for the Monte Carlo simulation is described in Figure 1b. The absorption and scattering coefficients of tissue mimicking used in the Monte Carlo simulation were retrieved from the literature (Figure 2). The anisotropy of scattering were taken to be 1, 1 and 0.9 at all wavelengths for water, gelatin and blood, respectively[10,16,17].

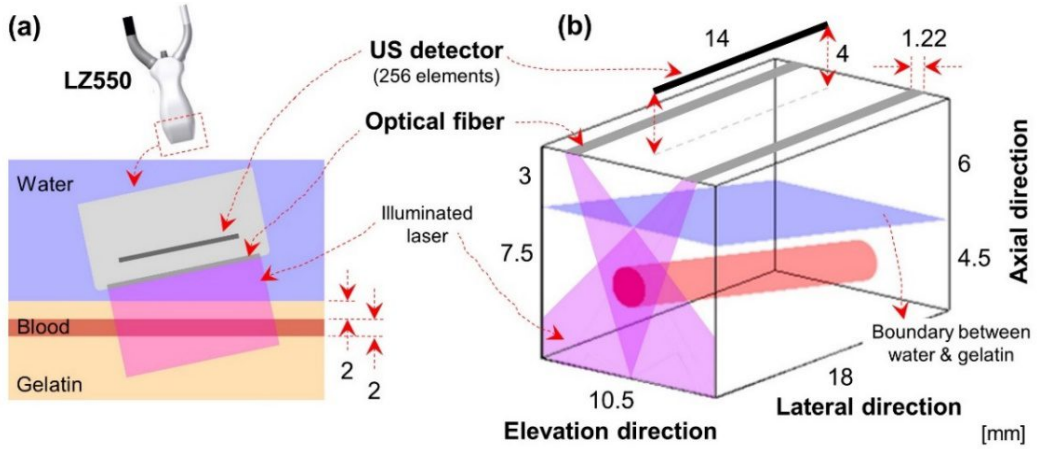

Figure 1. Experimental and theoretical structure. The lateral view (a) and 3-D structure (b) of PA imaging of blood flow. All dimensions are in mm.

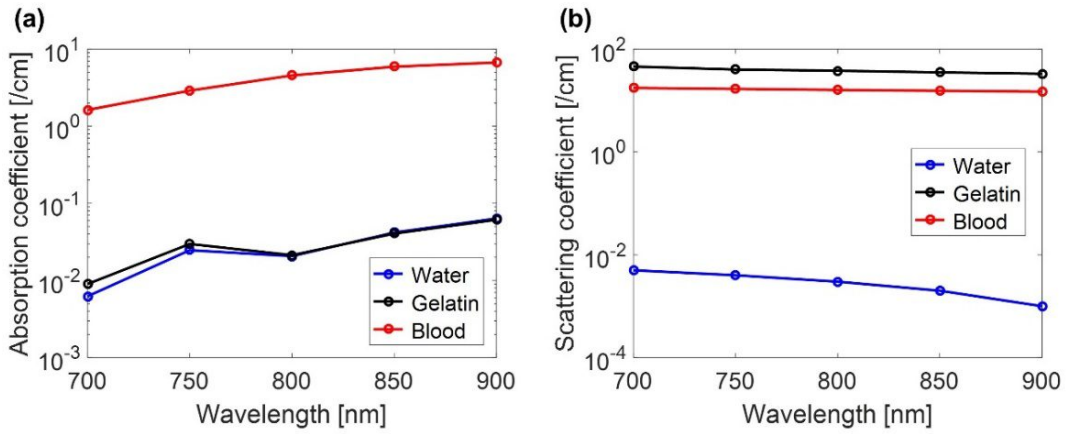

Figure 2. The absorption (a) and scattering (b) coefficients of tissue mimicking used in the Monte Carlo simulation[10,16,17].

2.3 RF spectroscopy analysis

The power spectrum of the PA signal was calculated using frequencies between 32-55 MHz, which correspond to the PA/US probe bandwidth. The normalized power spectra are fitted to a linear model with the least-squares method[6]. Two parameters of the linear model were extracted, the spectral slope (SS) and mid-band fit (MBF). The MBF is the magnitude of the linear fit at the center of the frequency interval.

3. RESULTS AND DISCUSSION

Representative profiles on the axial-elevation plane of fluence and energy deposition for 700 nm of the optical wavelength are shown in Figure 3. The axial distance starts from 4 mm, since the optical fibers were located at 4 mm below from the US detector. The divergent laser beams from two optical fibers crossed at 10 to 12 mm in the axial direction. The energy absorbed by the medium is shown in Figure 3b. The boundary between water and gelatin is located at a depth of 7 mm. The energy absorbed is proportionate to the absorption coefficient of the medium, so the energy absorbed by blood is much higher than those of water and gelatin.

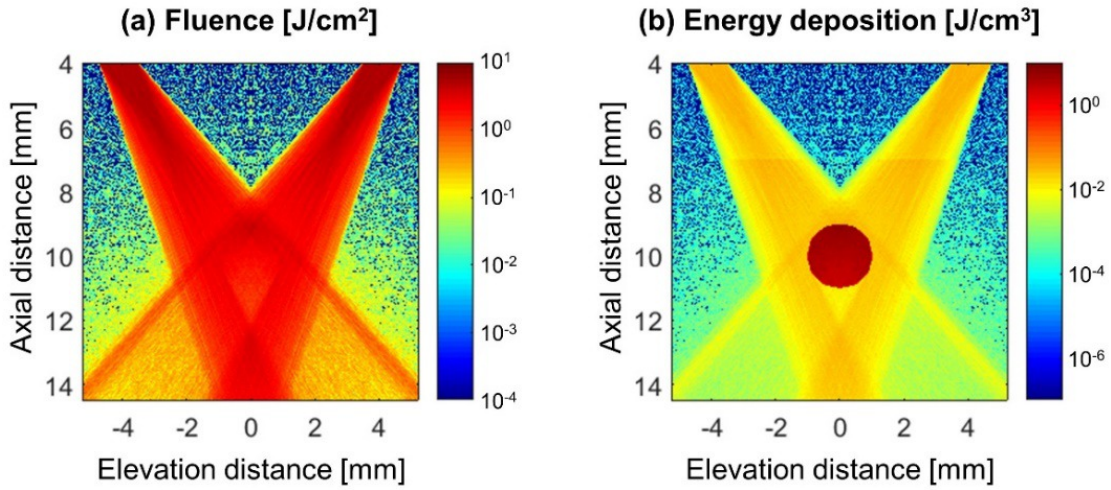

Figure 3. The Monte Carlo simulation at 0 mm of lateral direction (the first axial-elevation plane) for 700 nm. The axial distance starts from 4 mm, since the optical fibers are located at 4 mm below from the ultrasonic detector. (a) Fluence map and (b) energy deposition.

The PA maps were reconstructed using the 65th to 128th element (out of 256 elements) to maximize both the frame rate to 20 fps and the width of field of view, and to avoid the side-edge errors from the 1st and 256th elements, as shown in Figures 4a and 4d. The lateral distance was 3.5 mm, since the aperture length of the US detector was 14 mm. In the experimental PA map, the upper edge was observed at around 10 mm depth; however, the lower edge was not seen due to the low signal-to-noise ratio resulting from high frequency (40 MHz) ultrasound attenuation. This phenomenon can also be observed from the simulated RF signals shown in Figure 4b. On the other hand, the upper and lower edges were observed in the theoretical PA map as well as in the RF signals (Figures 4d and 4e). At the center of the lateral direction, the upper layer above the upper edge was folded because the blood vessel was not perpendicular to the transducer in the axial direction, and the corresponding PA signals were reconstructed by the delay-sum beamforming. The folded upper layer was dimly visible in the experimental PA map.

The experimental MBF increased with the optical wavelength as shown in Figure 4c (red curve). The MBF difference for the different wavelengths used was 10 dB. The MBF is a metric related to the PA signal amplitude, which is mainly determined by the molar extinction coefficient of oxyhemoglobin. This extinction coefficient increases with the optical wavelength in this setup[4]. The increase in the MBF with the illumination wavelength in the experimental results was similar with that in the theoretical results as shown in Figure 4f (red). The MBF difference for the wavelength range used was 8 dB in the theoretical results. The SS in ultrasound tissue characterization represents the effective size of scatterer[18–21]; it has also been shown to be related to the absorber size in PA imaging[7,22,23]. However, as observed in both the experimental and theoretical results in figures 4c and 4f (blue curves), respectively, the PA SS decreased with increasing illumination wavelength. This result was not expected since that the size of the RBC does not change as a function of wavelength. Therefore, the heating function $W(\mathbf{x})$ may have changed as different illumination wavelengths are used. We hypothesized that the optical fluence affects the SS since the fluence was dependent on the wavelength. The fluence changes as a function of illumination wavelength alter the heating function and therefore potentially the power spectrum of the RF signal. In other words, the perceived absorber size is due to fluence-induced changes in the heating pattern (and therefore the initial pressure $p_0(\mathbf{x})$, equation 2) that translates into changes in the frequency content of the RF signal recorded and simulated. This is similar to the spectral coloring and structural distortion studied by Beard *at al*[24]. Our group is investigating this interpretation further as it can play a role in interpreting PA RF spectroscopy results in the context of spectroscopic PA imaging of the blood flow.

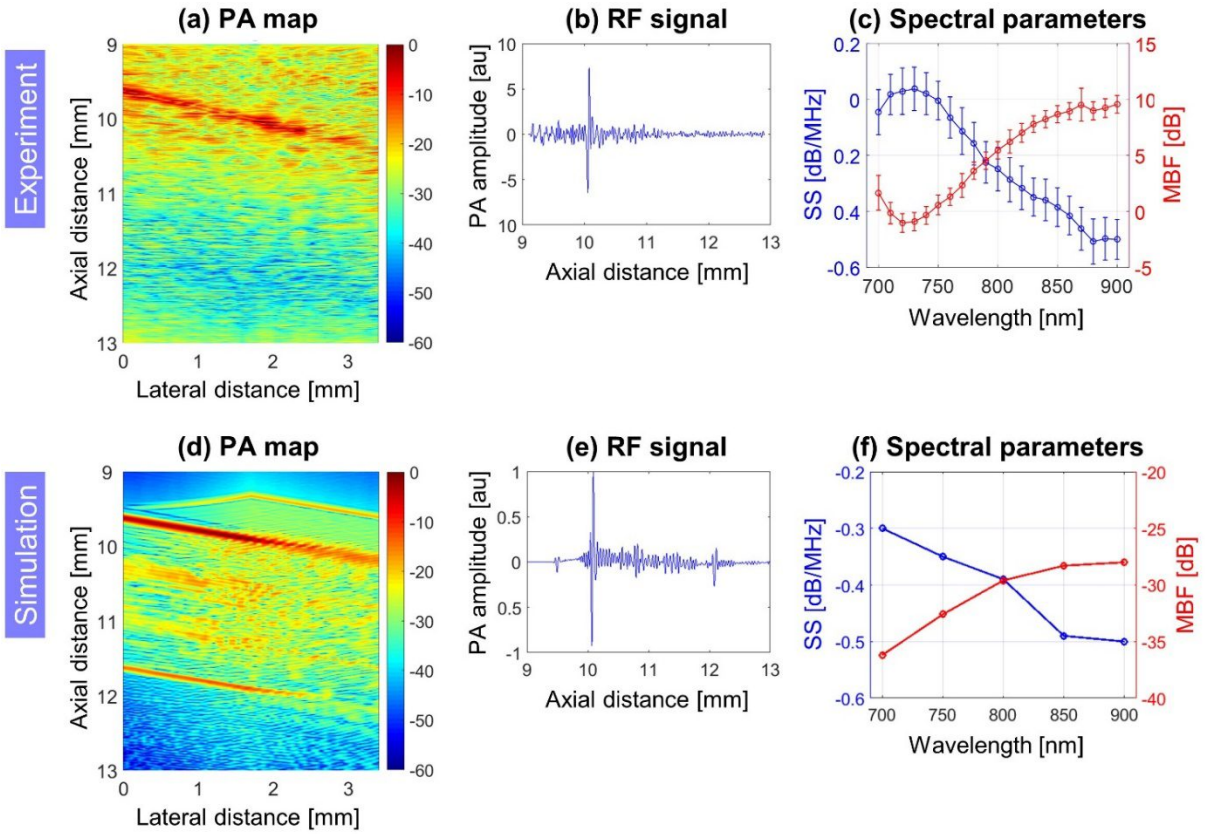

Figure 4. Experimental (upper) and theoretical (lower) results. (a) and (d) The PA map on the axial-lateral plane, reconstructed from 65th to 128th elements out of 256 elements, (b) and (e) the radio frequency signal at the center of the lateral direction, (c) and (f) the spectral parameters such as the spectral slope (SS, blue) and mi-band fit (MBF, red) plotted as a function of wavelength. The error bar indicates the magnitude of the cyclic variation in the spectral parameters, which is due to the cyclic variation in the PA signals under the pulsatile blood flow.

4. CONCLUSION

In this study, the experimental and theoretical PA effects of optical wavelength for the assessment of the pulsatile blood flow was investigated by means of quantitative RF spectroscopy parameters. The experimental MBF as well as the theoretical one increased with the optical wavelength, which was expected because the molar extinction coefficient of oxyhemoglobin increased with the illumination wavelength within the wavelength ranges studied. However, the experimental SS decreased with increasing wavelength even though the SS is sensitive to changes in the object size, which is wavelength-independent. In the theoretical simulations, the SS also decreased with increasing the wavelength, which was consistent with the experimental results. The SS decrease as a function of wavelength is not yet fully understood, however we speculate that it might be due to the effect of the fluence pattern, a wavelength-dependent parameter, has on the reconstruction of the PA images. In conclusion, the quantitative PA assessment of the pulsatile blood flow as a function of optical wavelength will help interpret *in-vivo* measurements of blood flow using PA imaging and should be further investigated.

ACKNOWLEDGMENTS

This work was funded by Natural Sciences and Engineering Research Council of Canada / Canadian Institutes of Health Research - Collaborative Health Research Projects grant # 462315-2014. Funding to purchase the equipment was provided by the Canada Foundation for Innovation, the Ontario Ministry of Research and Innovation, and Ryerson

University. E. Hysi is supported by a Vanier Canada Graduate Scholarship. We thank Elizabeth Berndl, and Graham Pearson at the Department of Physics at Ryerson University for providing technical support.

REFERENCES

[1] Diebold, G. J., "Photoacoustic Monopole Radiation: Waves from Objects with Symmetry in One, Two, and Three Dimensions," [Photoacoustic Imaging and Spectroscopy], L. V Wang, Ed., CRC Press, Boca Raton, FL, 3–17 (2009).

[2] Bok, T.-H., Hysi, E., Kolios, M. C., "Simultaneous measurement of erythrocyte aggregarion and oxygen saturation under in vitro pulsatile blood flow by high-frequency photoacoustics," 2014 IEEE Int. Ultrason. Symp. Proc., 1292–1295, Chicago, IL, USA (2014).

[3] Bok, T.-H., Hysi, E., Kolios, M. C., "Effect of optical wavelength on photoacoustic investigations of pulsatile blood flow," Proc. SPIE **9708**, A. A. Oraevsky and L. V. Wang, Eds., 97081M, San Francisco (2016).

[4] Bok, T.-H., Hysi, E., Kolios, M. C., "Simultaneous assessment of red blood cell aggregation and oxygen saturation under pulsatile flow using high-frequency photoacoustics," Biomed. Opt. Express **7**(7), 2769–2780 (2016).

[5] Xu, G., Meng, Z.-X., Lin, J. D., Yuan, J., Carson, P. L., Joshi, B., Wang, X., "The functional pitch of an organ: quantification of tissue texture with photoacoustic spectrum analysis," Radiology **271**(1), 248–254 (2014).

[6] Hysi, E., Saha, R. K., Kolios, M. C., "Photoacoustic ultrasound spectroscopy for assessing red blood cell aggregation and oxygenation," J. Biomed. Opt. **17**(12), 125006 (2012).

[7] Xu, G., Fowlkes, J. B., Tao, C., Liu, X., Wang, X., "Photoacoustic Spectrum Analysis for Microstructure Characterization in Biological Tissue: Analytical Model," Ultrasound Med. Biol. **41**(5), 1473–1480 (2015).

[8] Li, Q., Li, L., Li, Y., "Enhanced RBC aggregation in type 2 diabetes patients," J. Clin. Lab. Anal. **00**, 1–3 (2014).

[9] Yu, F. T. H., Amstrong, J. K., Tripette, J., Meiselman, H. J., Cloutier, G., "A local increase in red blood cell aggregation can trigger deep vein thrombosis: evidence based on quantitative cellular ultrasound imaging," J. Thromb. Haemost. **9**(3), 481–488 (2011).

[10] Jacques, S. L., Li, T., "Monte Carlo simulations of light transport in 3D heterogenous tissues (mcxyz.c)," <http://omlc.org/software/mc/mcxyz/index.html>.

[11] Wang, L. V, Jacques, S. L., Zheng, L., "MCML - Monte Carlo modeling of light transport in multi-layered tissues," Comput. Methods Programs Biomed. **47**(1995), 131–146 (1995).

[12] Keijzer, M., Jacques, S., "Light distributions in artery tissue: Monte Carlo simulations for finite-diameter laser beams," Lasers Surg. Med. **154**(1989), 148–154 (1989).

[13] Zalev, J., Kolios, M. C., "Detecting abnormal vasculature from photoacoustic signals using wavelet-packet features," Proc. SPIE **7899**, 78992M (2011).

[14] Zalev, J., Kolios, M. C., "Exact solution for a photoacoustic wave from a finite-length cylindrical source," J. Acoust. Soc. Am. **137**(4), 1675–1682 (2015).

[15] Cox, B. T., Beard, P. C., "Fast calculation of pulsed photoacoustic fields in fluids using k-space methods," J. Acoust. Soc. Am. **117**(6), 3616 (2005).

[16] Jacques, S. L., "Optical properties of biological tissues: a review," Phys. Med. Biol. **58**(11), R37–R61 (2013).

[17] Smith, R. C., Baker, K. S., "Optical properties of the clearest natural waters (200-800 nm)," Appl. Opt. **20**(2), 177–184 (1981).

[18] Baddour, R. E., Sherar, M. D., Kolios, J. W. H. J. C. C., Baddour, R. E., Sherar, M. D., Hunt, J. W., "High-frequency ultrasound scattering from microspheres and single cells," J. Acoust. Soc. Am. **117**(2), 934–943 (2005).

[19] Lizzi, F. L., Ostromogilsky, M., Feleppa, E. J., Rorke, M. C., Yaremko, M. M., "Relationship of Ultrasonic Spectral Parameters to Features of Tissue Microstructure," IEEE Trans. Ultrason. Ferroelectr. Freq. Control **34**(3), 319–329 (1987).

[20] Lizzi, F. L., Feleppa, E. J., Alam, S. K., Deng, C. X., "Ultrasonic spectrum analysis for tissue evaluation," Pattern Recognit. Lett. **24**(4-5), 637–658 (2003).

[21] Kolios, M. C., Czarnota, G. J., Lee, M., Hunt, J. W., Sherar, M. D., "Ultrasonic spectral parameter characterization of apoptosis," Ultrasound Med. Biol. **28**(5), 589–597 (2002).

[22] Xu, G., Dar, I. A., Tao, C., Liu, X., Deng, C. X., Wang, X., "Photoacoustic spectrum analysis for microstructure characterization in biological tissue: A feasibility study," Appl. Phys. Lett. **101**(22), 221102 (2012).

[23] Hysi, E., Dopsa, D., Kolios, M. C., "Photoacoustic tissue characterization using envelope statistics and ultrasonic

spectral parameters," Proc. SPIE **8943**, 89432E (2014).
[24] Cox, B., Laufer, J. G., Arridge, S. R., Beard, P. C., "Quantitative spectroscopic photoacoustic imaging : a review," J. Biomed. Opt. **17**(6), 061202 (2012).